Microseismic evidence of slip partitioning for the Rudbar-Tarom earthquake (Ms 7.7) of 1990 June 20 in NW Iran

M. Tatar, Denis Hatzfeld

Geophys. J. Int. (2009) **176,** 529–541 doi: 10.1111/j.1365-246X.2008.03976.x

Microseismic evidence of slip partitioning for the Rudbar-Tarom earthquake (M_s 7.7) of 1990 June 20 in NW Iran

M. Tatar[1,2] and D. Hatzfeld[1]

[1] *Laboratoire de Géophysique Interne et Tectonophysique, CNRS, Université Joseph Fourier, Maison des Géosciences,* BP 53, 38041 *Grenoble Cedex* 9*, France*
[2] *International Institute of Earthquake Engineering and Seismology,* PO Box 19395/3913*,Tehran, Iran. E-mail: denis.hatzfeld@ujf-grenoble.fr*

Accepted 2008 September 12, Received 2008 September 11; in original form 2007 December 12

SUMMARY

The focal mechanism of the destructive earthquake at Rudbar in northern Iran on 1990 June 20 was an unexpected left-lateral strike-slip motion on a previously unknown fault, the Baklor–Kabateh–Zard-Goli fault, within a complex system of reverse faults. We analysed microseismicity recorded by a dense local network deployed for 7 weeks, 8 yr after the main shock, to help evaluate the subsurface geometry and kinematics of the active fault system. In the west, the 1998 microseismicity seems to be related to the reverse Manjil. In the centre, we observe both reverse faulting associated to the Manjil fault and strike-slip faulting associated with de Zard-Goli rupture whose dip progressively changes from 45°N to vertical. In the east, the reverse faulting is located south of the Manjil fault and strike-slip faulting to the vertical Zard-Goli fault. We suggest that because the only stable geometry that accommodates large partitioning motion prevents the strike-slip fault to intersect the reverse fault, the active reverse fault jumps southwards beneath the Shahrud fault.

Key words: Earthquake source observations; Seismicity and tectonics; Continental neotectonics; Dynamics: seismotectonics.

INTRODUCTION

Slip partitioning of oblique convergence onto parallel strike-slip and thrust faults with orthogonal slip vectors is a common feature in active tectonics, especially for large finite deformation in oblique subduction zones (e.g. Fitch 1972; McCaffrey 1992). In continental tectonics, we also observe such partitioning (e.g. Mount & Suppe 1987). Strike-slip and reverse motion may occur on two parallel faults at all scale length (Lettis & Hanson 1991). Slip partitioning is a more stable fault system, especially in orientation of the faults, that can accommodate large-scale oblique motion across a distributed deformation zone (McKenzie & Jackson 1983), but the reason it initiates has been a matter of debate. Richard & Cobbold (1989) conducted analogue modelling suggesting that a lower ductile layer is necessary for partitioning. Michael (1990) suggested that the energy released onto two separate faults is less than on a single oblique fault, but this argument is discussed by Molnar (1992) who suggested, among other authors (e.g. Zoback *et al*. 1987; Jones & Tanner 1995; Norris & Copper 2001), that the main reason for slip partitioning is the presence of a pre-existing weak fault. Other suggestions have been proposed of factors that favour partitioning, such as the minimization of work against friction (Jones & Wesnousky 1992) or the degree of obliquity of the motion (Teyssier *et al*. 1995) or the angle of dip of the strike-slip fault (Norris & Cooper 2001). The geometry at depth of the two faults is also a matter of debate. If the strike-slip fault located in the hangingwall of the reverse fault intersects the later one, the partitioning system is not stable and cannot accommodate large motion.

One of the most destructive modern Iranian earthquakes, the Rudbar-Tarom earthquake ($M_s \sim 7.7$), occurred on 1990 June 20, between Tabriz and Gazvin, in the western part of the Alborz mountain belt, south of the Caspian Sea. It occurred in an area with no detailed record of historical seismicity (Berberian *et al*. 1992). Very little is known about the geometry and mechanism of the faulting in this area although three main fault segments with a total length of 80 km, arranged in a right-stepping en-échelon system, were reported as showing co-seismic surface faulting. The WNW–ESE left-lateral strike-slip focal mechanism, unexpected in this area where reverse mechanisms dominate, was interpreted as partitioning due to the oblique convergence in the Alborz mountains (Berberian *et al*. 1992; Gao & Wallace 1995).

Because of the lack of a local seismological network, no precise information was available regarding the location of the main shock and of the aftershock sequence nor of the detailed geometry of the active faults.

In this paper, we precisely analyse the microseismicity located near the Rudbar fault system in 1998, 8 yr after the main shock, in an attempt to elucidate the characteristics of the faulting related to this complex earthquake and to investigate the partitioning of oblique convergent motion. We are aware that microseismicity is due to small ruptures on small faults, related or not to large faults. Because we know how questionable the interpretation of microseismicity is,

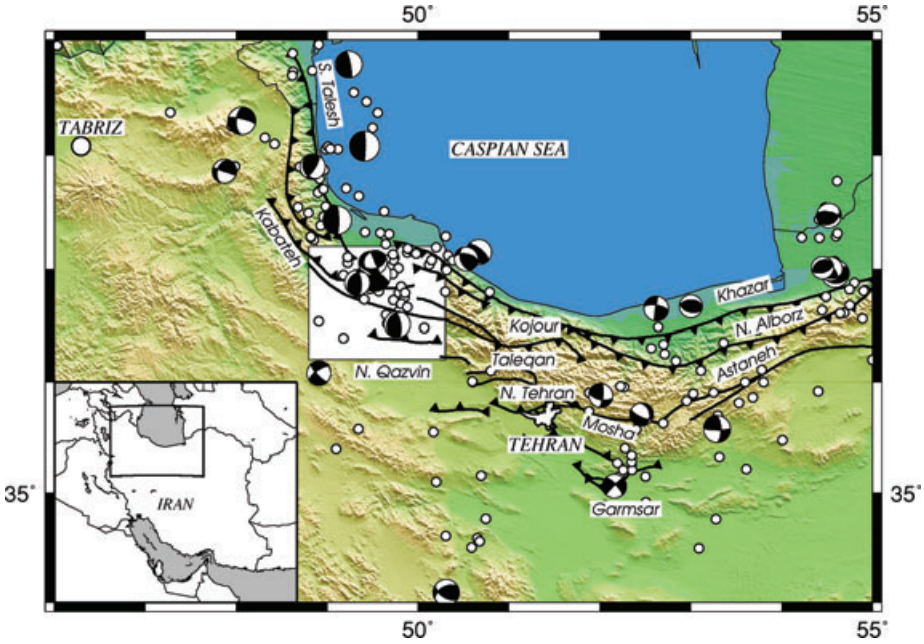

Figure 1. Tectonic map of Central Alborz. Faults are from Berberian & Yeats (1999, 2001) and Allen *et al*. (2003). Seismicity (Engdahl *et al*. 1998; $M_b > 4.5$) is shown by open circles. CMT focal mechanisms (http://www.seismology.harvard.edu/CMTsearch.html) are reported as black focal sphere. The white rectangle is the location of the Rudbar region.

we try to present the data and the interpretation in a way the reader can make his own decision. The 1990 Rudbar-Tarom earthquake was the most destructive earthquake in Iran in the last century, and any information it reveals is relevant for understanding the tectonics of the area.

TECTONIC AND SEISMICITY SETTING

The Alborz range that bounds the southern edge of the South Caspian Sea is approximately 600 km long and 100 km wide (Fig. 1). It consists mainly of late Precambrian to Eocene sedimentary and volcanic rocks (Stöcklin 1974). The geological structures in this mountain range are produced by late Cenozoic shortening and are parallel to the range (Alavi 1996). Several active faults affect the Central Alborz and accommodate the present-day oblique convergence across the mountain range (Berberian *et al*. 1992; Trifonov *et al*. 1996; Allen *et al*. 2003). Most of the faults located to the north of the Central Alborz range dip southwards, whereas most of the faults located on the south side dip northwards but this is not so clear west of the Sefi-Rud river (Stöcklin 1974). The pre-Pliocene tectonics involved a transpressional regime (Axen *et al*. 2001) which was followed by a more recent partitioning between pure reverse faulting and left-lateral strike-slip motion affecting the Alborz as a whole (Jackson *et al*. 2002; Allen *et al*. 2003). Based on GPS motion, the present-day shortening across the Central Alborz is about 5 ± 2 mm yr^{-1} associated with a left-lateral shear of 4 ± 2 mm yr^{-1} (Vernant *et al*. 2004b).

Although the Central Alborz has suffered from several destructive earthquakes, the only known historical events near the Rudbar-Tarom epicentral area were in 1485 (M_s 7.2) and 1608 (M_s 7.6) which occurred several tens of kilometres away (Ambraseys & Melville 1982).

Prior to 1990, the instrumentally recorded seismic activity in the area was relatively sparse and of moderate magnitude (Berberian *et al*. 1992): in 1905 ($M_s \sim 6.2$), 1948 ($M_b \sim 5.5$), 1968 ($m_b \sim 4.7$), 1970 ($m_b \sim 4.5$), 1980 ($m_b \sim 4.1$), 1983 ($m_b \sim 5.6$) and 1990 ($m_b \sim 3.9$) some of which are shown in Fig. 2. The lack of a local or regional seismological network, in addition to the poor knowledge of the crustal velocity structure beneath the Alborz mountain range, did not allow precise determination of earthquake source parameters, and earthquake locations were only accurate to within a few tens of kilometres. With this uncertainty, it is not possible to relate the catalogued seismicity to particular active faults (Engdahl *et al*. 1998).

THE RUDBAR-TAROM EARTHQUAKE

On 1990 June 20, an earthquake of M_s 7.7 (M_w 7.3) occurred in the area of Rudbar, which is located between Tabriz and Gazvin (Fig. 2). It killed more than 40 000 people, injured 60 000 and destroyed more than 700 villages over a 120-km-long area. It is the most destructive documented earthquake of the last century in Iran. The epicentre was located in a region of high topography, and caused several landslides. A first survey of the area (Moinfar & Naderzadeh 1990) probably misidentified landslides located south of the Manjil basin as surface ruptures (Fig. 2). Surface ruptures were not located on known active faults such as the Manjil, the Deylaman and the Poshtkuh major reverse faults but the earthquake ruptured three different and previously unknown fault segments: the Baklor segment in the west, the Kabateh segment in the centre and the Zard-Goli segment in the east, arranged in an en-échelon system striking WNW–ESE on average. The motion was left-lateral on the western Baklor segment and transpressional (95 cm of offset and 60 cm of left-lateral motion) on both the Kabateh and Zard-Goli segments on a nearly vertical or steeply SSW-dipping fault planes, and therefore dips in the opposite sense to the local topography for Baklor and Kabateh faults (Berberian *et al*. 1992).

Some authors suggested that the 1990 earthquake filled the seismic gap between the 1485 and the 1608 earthquakes in the east and the 1896 earthquake in the west, although the fault system between

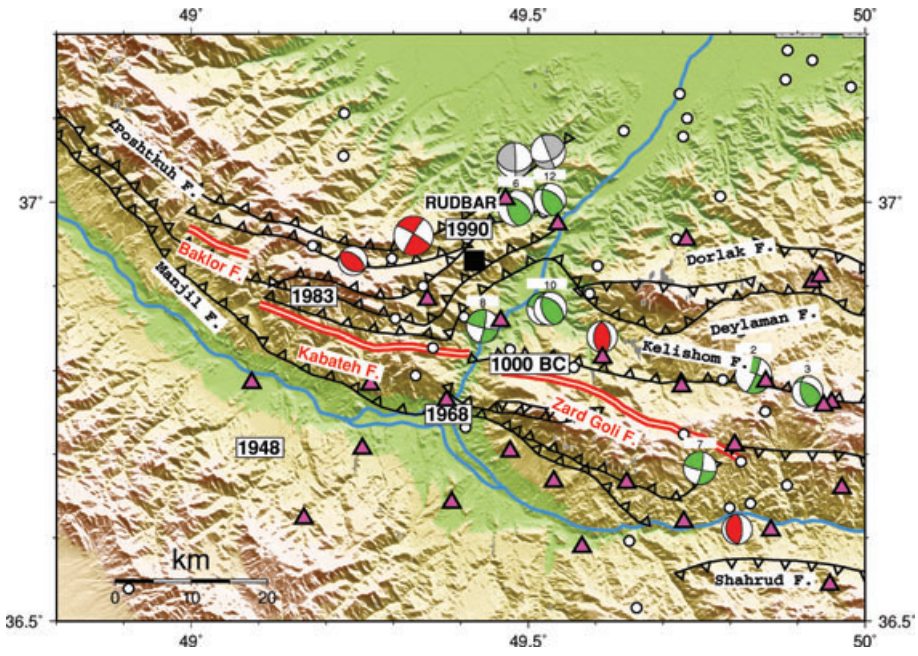

Figure 2. Tectonic map of the Rudbar region. Faults are from Berberian *et al*. (1992). The co-seismic surface rupture is plotted as a double red line. The pink triangles are the seismological stations. The numbers are the dates and approximate epicentres of the historical earthquakes from Ambraseys & Melville (1982) and Berberian (1994). Modelled mechanisms (Jackson *et al*. 2002) are red spheres, aftershock mechanisms are green spheres (Gao & Wallace 1995), and CMT (see Fig. 1) are grey spheres. The black square is the city of Rudbar. Note the large variety of mechanisms for the early aftershocks of magnitude ranging between 4.6 and 7.7.

the two areas is rather complex and discontinuous (Berberian *et al*. 1992). Others (Hamzehloo *et al*. 1997b) suggested that the earthquake was the result of the Sefid-Rud dam impoundment, 100 m high, filled in 1962.

The well-determined strike-slip mechanism (left-lateral on a 288°N striking plane dipping vertically) was unexpected because of the reverse faulting associated with most of the faults in this area (Gao & Wallace 1995). The aftershocks that occurred over the following days showed a mixture of strike-slip and reverse motion on a plane trending consistently NW–SE for most of them (Fig. 2). Among the 12 mechanisms computed, five are left-lateral strike-slip on a plane trending ∼285°, and six are reverse faulting on a plane trending ∼304° and dipping north at ∼50°. One reverse mechanism shows an active plane trending different at 25°. If the slip vectors trend differently, depending on the type of mechanism, the shortening *P*-axis direction points consistently NE (Gao & Wallace 1995). The strike-slip mechanisms for the main shock and the reverse faulting aftershocks, were thought to signify slip partitioning of oblique convergence between Central Iran and the Caspian Sea (Berberian *et al*. 1992; Jackson 1992) on two different faults striking parallel.

Body wave modelling of the main shock (Campos *et al*. 1994) indicated a first bilateral rupture for 10 s that was followed by an eastward rupture propagation which released most of the seismic moment 40 km east of the epicentre. The focal mechanisms of the different pulses show a consistent pattern of left-lateral strike-slip faulting on a plane striking 295°–330° and dipping ∼78°–99° NE at a depth of ∼4–14 km, consistent with the surface observations, having in mind the associated uncertainties. This model of rupture propagation is, therefore, consistent with an initiation on the eastern part of the Baklor fault (or the western part of the Kabateh fault), and with the maximum slip being released on the Zard-Goli fault.

DATA AND PROCEDURE

In 1998 June and July, we deployed a temporary network of 30 portable seismological stations over the Rudbar region (Fig. 2). Twenty-five instruments were digital recorders (TAD) connected to a 2 Hz Mark-Product L22 vertical seismometer. Five digital continuously recording data loggers (Reftek) were connected to four 2-Hz Mark-Product, and to one broad-band Guralp CMG-40T seismometers. All stations had a sampling rate of 100 Hz.

Because we have no previous information about the velocity structure, we follow the procedure already used for other areas in Iran (Tatar *et al*. 2004; Yaminifard *et al*. 2006). The approach is based on a simultaneous inversion for a 1-D velocity structure and hypocentres based on the VELEST programme (Kissling 1988). Using a selected set of 249 events [$N > 10$ stations, root-mean-square (rms) < 0.1 s, ERH and ERZ uncertainties <1 km and an azimuthal gap $<180°$], we compute a mean V_p/V_s ratio of 1.725 ± 0.002 with a total of 3590 arrival times.

Second, we search for an appropriate local velocity model. To ensure a reasonable convergence of the results, we explore 50 initial models by introducing random changes up to 0.5 km s^{-1} in the velocity for each layer. Initially, we assume a multilayered velocity structure composed of nine layers of uniform velocity 5.9 km s^{-1}, 2 km thick, from the surface to a depth of 18 km, to locate the major interfaces. The result suggests that only three layers are required. Then, merging the layers of similar velocity, we start with a three-layer initial model, that is, again randomly perturbated as described above. The model we obtained is then used as a starting model.

The final result indicates a very good convergence for more than 80 per cent of the starting models to a simple three-layer velocity model for the upper crust above the earthquake hypocentres. A receiver-function analysis (Langston 1979; Liggoria & Ammon 1999) of three teleseismic events recorded on the broad-band

Table 1. Velocity structure.

Top of the layer (km)	Velocity (km s^{-1})
0	5.4
6	5.9
14	6.3
35	8.2

seismograph was used to constrain both the *S*-wave velocity in the lower crust and to determine the depth of Moho (Tatar 2001).

The final model (Table 1) has a crustal thickness of 35 ± 2 km and consists of a ∼6-km-thick sedimentary layer above an 8-km-thick crystalline upper crust, which overlies a slow 21-km-thick lower crystalline crust. This velocity structure is consistent with the results obtained by Mangino & Priestly (1998), Ashtari *et al*. (2005), Sodoudi *et al*. (2004) in the same area.

RESULTS

Earthquake location

We located a total number of 410 events (magnitude ranging between 1 and 4) recorded by a minimum of four stations (Fig. 3). The seismicity defines an elongated pattern approximately 80 km long, trending WNW–ESE and surrounding two of the segments that ruptured during 1990 (Kabateh and Zard-Goli). Most earthquakes are located slightly north of the 1990 surface ruptures and it is not possible to relate univocally all microearthquakes to individual faults observed at surface and some clusters are more diffused than others. Indeed, aftershocks microseismicity, 8 yr after the Rudbar-Tarom earthquake, might be related to a complex stress pattern surrounding the main fault but not to the motion of the active fault itself. We will examine this aftershock seismicity, both in maps and cross-sections, in an attempt to improve our knowledge of this destructive earthquake.

To resolve better the pattern of the aftershocks, we first selected the 276 earthquakes whose locations are constrained by at least eight arrival times (including one *S*), with an rms residual less than 0.12 s, horizontal (ERH) and vertical (ERZ) uncertainties smaller than 1 km and an azimuthal gap smaller than 180°. Then, to reduce the possible scatter due to local heterogeneities in the velocity structure, we relocated the earthquakes relative to each other within a cluster using the double-difference method HypoDD (Waldhauser & Ellsworth 2000). We used pairs of events with minimum of eight links (traveltimes to stations) and located less than 10 km apart.

Both the Hypo71 selection (Fig. 3) and the HypoDD locations (Fig. 4) confirm that the seismic activity is concentrated near the Zard-Goli and Kabateh ruptures, but the microearthquakes are not obviously associated with the outcrops of the Manjil, Poshtkuh, Deylaman or Kelishom faults. Most of the seismicity is located north of the co-seismic surface ruptures, between the surface and a depth of 16 km, indicating a probable northward dip of the faults; in disagreement with the surface observations of Berberian *et al*. (1992), which showed mainly a vertical or steep southward dip. Earthquakes are located south of the Manjil fault only at the eastern termination of the Zard-Goli rupture. The pattern of seismicity seems simpler, but also less active, around the Kabateh rupture than around the Zard-Goli rupture. A dense cluster of earthquakes is located between the Kabateh and Zard-Goli ruptures, near the Sefid-Rud river. Another cluster is located at the eastern end of the Zard-Goli fault. The area covered by the seismicity is consistent

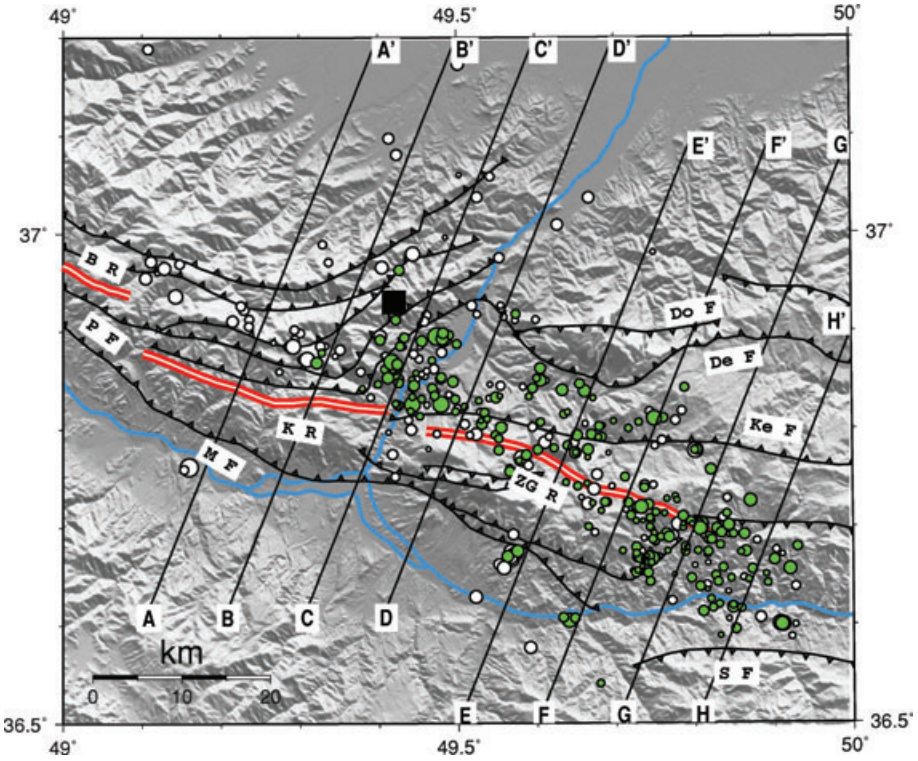

Figure 3. Location of all 470 earthquakes recorded by a minimum of four stations (white circles). The green circles are the 276 selected earthquakes whose location is constrained by at least eight arrival times (including one *S*), with an rms < 0.12 s, ERH and ERZ < 1 km and an azimuthal gap < 180°. The location of eight cross-sections is shown. Abbreviations for the faults are: BR, Baklor rupture; De, Deylaman; Do, Dorlak; K R, Kabateh rupture; Ke, Kelishom; P, Poshtkuh; S, Shahrud; ZG R, Zard-Goli rupture

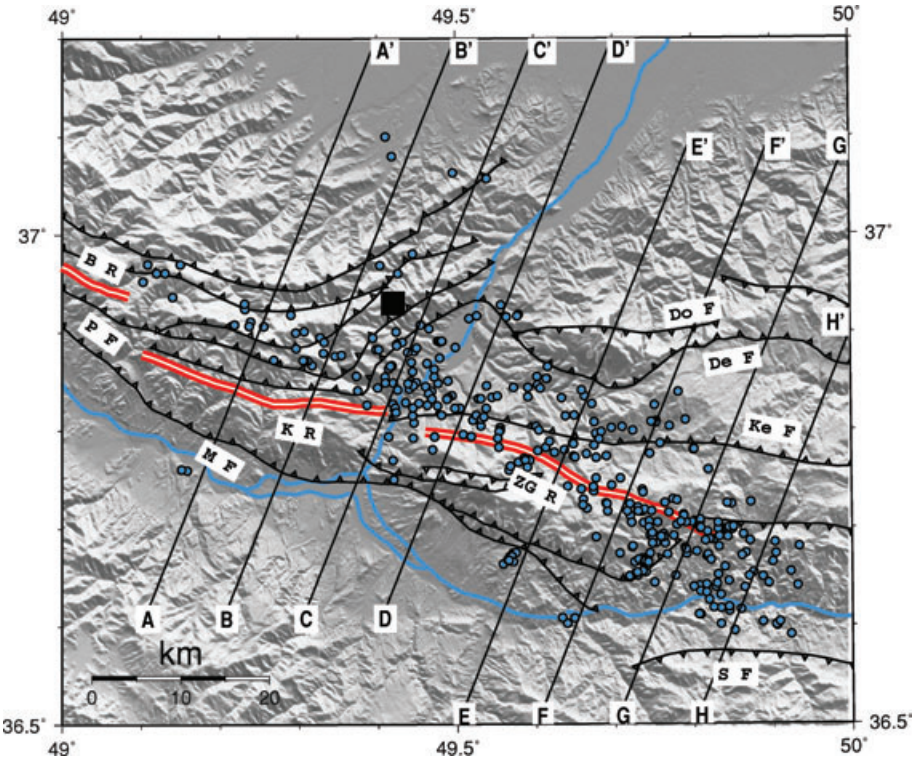

Figure 4. Relocated seismicity using the double-difference method (Waldhauser & Ellsworth 2000) with eight links and distance between pairs of 10 km.

with a fault surface of ~80 × 20 km^2, and therefore a seismic moment in the range ~8.8 × 10^{19}–1.4 × 10^{20} Nm computed by different authors assuming a rigidity of 3 × 10^{10} Nm^{-2} and an average slip of 2.4 m (Berberian *et al*. 1992; Campos *et al*. 1994; Gao & Wallace 1995).

Depth distribution

Fig. 5 shows a histogram of the depth distribution of both all earthquakes and of the selected set of earthquakes located during the experiment. The pattern of earthquakes is comprised between the surface and 19 km with a maximum of earthquakes at depths ranging between 8 and 16 km. These depths are shallower than the depths observed for the 2004 Baladeh aftershocks in Central Alborz (Tatar *et al*. 2007) which were ranging between 11 and 30 km. But they are similar to what is generally observed in Iran and especially what was observed during a microearthquake survey conducted around Tehran (Ashtari *et al*. 2005). Teleseismic locations (Engdahl *et al*. 2006) or body waves modelling of strong earthquakes report depth greater than 20 km around the Talesh, located west of the Caspian Sea, or associated with the trans-Caspian Apscheron-Balkan sill (Jackson *et al*. 2002). But these deeper events are all associated with major (crustal or even lithospheric) discontinuities involving the crust of the Caspian Sea. It seems, therefore, that the earthquakes occurring in an intracontinental setting (Zagros, Rudbar or Tehran) are classically restricted to the brittle upper crust whereas those related to the Caspian crust are deeper. Moreover, in the case of Rudbar, the 1990 centroid depth was estimated to be 11.7 km (Campos *et al*. 1994), and therefore in the middle of the depth distribution suggesting that the rupture initiated in the middle of the fault zone as it has been observed for the Baladeh event (Tatar *et al*. 2007) rather than at the edge as for the Bam earthquake (Tatar *et al*. 2005).

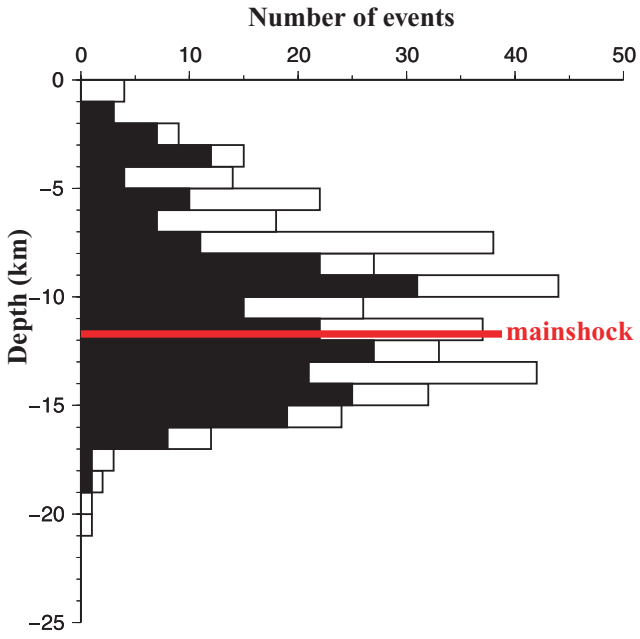

Figure 5. Depth distribution of the aftershocks plotted as a histogram showing both the selected set of events in black and all events in white. The centroid depth of the main shock (Campos *et al*. 1994) is indicated by the red line.

Focal mechanisms

We computed (Fig. 6, Table 2 and supporting information Appendix S1) 52 mechanisms of quality A (three quadrants sampled, 10 reliable polarities and the two nodal planes constrained within 20°) and 17 of quality B (two quadrants sampled and less

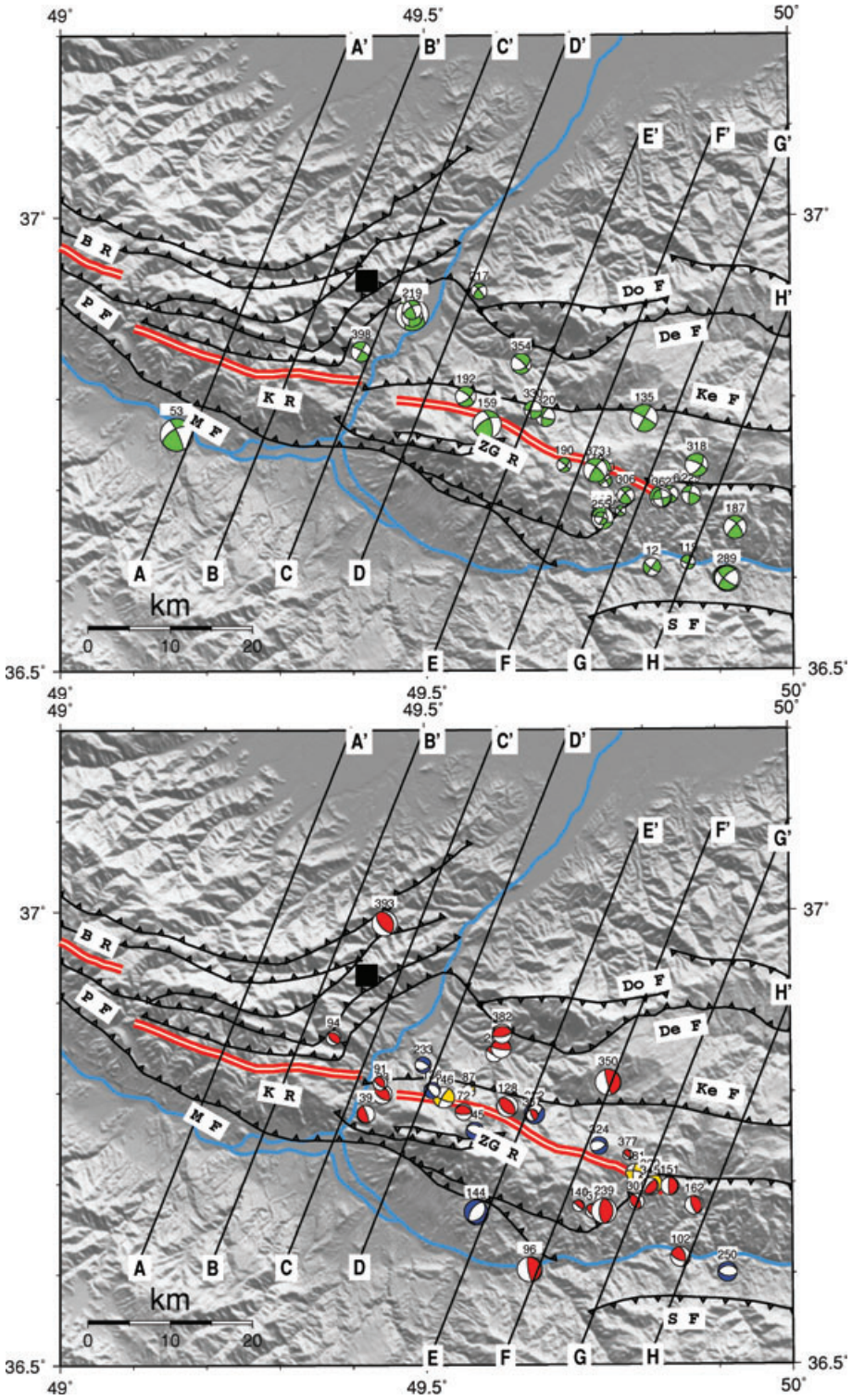

Figure 6. Map of the focal mechanisms (equal-area lower hemisphere). (a) Left-lateral mechanisms (in green) on E–W to NW–SE striking planes; (b) other mechanisms with reverse (in red), normal (in blue) and right-lateral (in orange). The great variety of mechanisms is similar to the early aftershock mechanisms reported in Fig. 2.

than 10 reliable polarities). Most of them show either strike-slip or reverse faulting, as was observed for the 1990 main shock and aftershocks (Gao & Wallace 1995). We report on two different maps the left-lateral strike-slip mechanisms similar to the 1990 main shock (Fig. 6a) and all others mechanisms (Fig. 6b). There is no clear geographical pattern distribution between reverse and strike-slip mechanisms which does not help to discriminate the motion on active faults and precise partitioning. A few normal-faulting mechanisms (136, 142, 143, 145, 233, 235, 250, 322 and 324) are also seen and are spread all over the area.

Table 2. Parameters of the focal mechanisms.

N	Date	Time	Lat	Lon	*z*	Mag	Az1	pl1	de1	Az2	pl2	de2	Azp	dep	Azt	det	Im	Q
12	980613	19:41	36.61	49.80	10	2.0	125	75	179	35	89	0	81	10	349	10	1	A
26	980614	22:48	36.71	49.72	9	1.7	305	70	−14	40	76	−159	263	24	171	4	−1	B
33	980615	16:04	36.79	49.44	7	2.2	320	36	102	125	54	81	221	9	3	78	1	B
35	980615	20:10	36.67	49.76	11	1.2	130	85	−11	221	78	−174	85	11	175	4	−1	B
37	980615	22:09	36.66	49.72	15	1.7	335	44	112	125	50	69	229	3	330	74	1	A
39	980616	00:29	36.77	49.41	14	2.0	340	80	91	150	10	80	68	35	252	55	1	B
44	980616	13:08	36.66	49.74	15	2.4	285	84	179	15	89	0	240	4	149	4	−1	A
53	980616	23:16	36.76	49.15	16	3.7	335	81	29	240	61	169	104	13	201	26	1	A
72	980618	03:20	36.77	49.55	6	1.9	295	27	112	90	65	78	188	19	338	67	1	A
87	980619	00:50	36.80	49.55	11	1.4	15	60	19	275	73	148	327	8	231	33	1	A
91	980619	09:37	36.81	49.43	10	1.5	340	35	119	125	60	70	228	13	355	68	1	B
94	980619	17:32	36.86	49.37	11	1.7	295	32	72	135	59	100	217	14	71	73	1	A
96	980619	20:08	36.60	49.64	15	2.8	170	80	90	350	10	90	260	35	80	55	1	B
102	980620	04:50	36.61	49.84	14	2.2	350	49	138	110	60	49	227	6	326	54	1	A
119	980622	01:39	36.61	49.85	13	1.6	105	75	18	10	72	164	237	2	328	23	1	A
120	980622	20:30	36.70	49.74	13	1.5	325	78	179	235	89	0	280	8	189	8	1	A
128	980624	21:20	36.78	49.61	14	2.4	320	45	93	135	45	86	227	0	318	87	1	A
135	980626	12:46	36.77	49.79	4	3.1	300	85	179	30	89	0	255	3	164	3	−1	A
136	980626	14:20	36.80	49.50	10	1.8	145	65	−73	290	29	−121	84	66	222	18	−1	A
140	980627	23:56	36.67	49.70	14	1.3	130	81	90	310	9	90	220	36	40	54	1	B
142	980628	07:03	36.66	49.74	13	1.6	290	72	−29	30	61	−159	247	33	341	6	1	A
143	980628	07:47	36.66	49.56	4	2.6	25	35	−90	205	55	−90	115	80	295	10	−1	B
144	980628	07:53	36.66	49.56	4	2.6	45	35	−81	215	55	−95	103	78	309	10	−1	B
145	980628	19:18	36.75	49.56	11	1.9	110	60	−90	290	30	−90	20	75	200	15	−1	A
146	980628	20:18	36.79	49.52	9	2.4	115	70	165	210	76	20	341	4	73	24	1	A
148	980629	03:37	36.89	49.48	12	3.7	310	53	24	205	71	140	261	11	161	40	1	A
151	980629	04:01	36.69	49.83	15	2.0	180	80	90	360	10	90	270	35	90	55	1	B
152	980629	04:32	36.89	49.48	12	2.4	300	50	22	195	72	137	252	14	149	41	1	A
159	980630	08:04	36.77	49.58	9	3.2	345	64	31	240	62	150	112	1	203	39	1	A
162	980701	05:34	36.67	49.86	16	2.1	160	70	90	340	20	90	250	25	70	65	1	A
176	980703	13:22	36.71	49.73	12	1.7	170	85	179	260	89	0	125	3	34	3	−1	A
187	980705	02:47	36.65	49.92	14	2.6	320	65	11	225	79	154	274	9	180	25	1	A
190	980706	02:19	36.72	49.68	8	1.6	310	80	−26	45	63	−168	264	25	360	11	−1	A
192	980706	14:51	36.80	49.55	12	2.3	310	70	−27	50	64	−157	268	33	1	3	−1	A
198	980708	06:30	36.66	49.74	14	2.5	110	70	27	10	64	157	239	3	331	33	−1	A
208	980710	03:55	36.84	49.59	15	1.9	120	80	90	300	10	90	210	35	30	55	1	B
217	980711	01:17	36.91	49.57	6	1.8	320	79	24	225	65	167	90	8	184	25	1	A
219	980711	03:59	36.89	49.48	12	2.1	335	80	26	240	63	168	105	11	200	25	1	A
229	980712	01:12	36.69	49.86	10	2.1	285	71	15	190	75	160	238	3	146	23	1	A
231	980712	07:36	36.84	49.60	15	2.2	100	80	90	280	10	90	190	35	10	55	1	B
233	980712	18:19	36.83	49.49	12	1.8	70	40	−132	300	61	−60	256	61	9	11	−1	A
239	980713	02:09	36.66	49.74	14	2.9	0	30	90	180	60	90	270	15	90	75	1	A
248	980714	09:30	36.60	49.90	8	2.6	315	70	0	225	89	179	178	14	271	14	1	B
249	980714	10:44	36.60	49.91	9	3.0	125	73	−31	225	60	−160	81	33	177	8	−1	B
250	980714	10:59	36.60	49.91	8	2.2	100	55	−78	260	36	−106	48	76	181	9	−1	A
255	980715	23:42	36.66	49.73	14	1.4	285	75	−18	20	72	−164	242	23	332	2	−1	B
268	980717	18:45	36.72	49.74	14	2.1	105	85	179	195	89	0	60	3	329	3	−1	A
281	980718	20:27	36.71	49.78	11	2.0	280	75	−161	185	72	−15	143	23	52	2	−1	A
289	980719	20:45	36.60	49.91	10	2.7	130	75	−18	225	72	−164	87	23	177	2	−1	A
296	980720	10:31	36.69	49.83	16	1.9	305	80	26	210	63	168	75	11	170	25	1	A
301	980721	02:33	36.67	49.78	16	1.8	330	55	95	140	35	81	55	9	262	79	1	A
306	980721	05:29	36.69	49.77	8	1.9	320	78	22	225	67	167	91	7	184	24	1	A
318	980722	07:44	36.72	49.87	11	2.6	295	73	−31	35	60	−160	251	33	347	8	−1	A
320	980722	13:42	36.77	49.66	13	2.1	105	80	179	195	89	0	60	7	329	7	−1	A
322	980722	22:32	36.77	49.64	12	2.3	230	25	−90	50	65	−90	320	70	140	20	−1	A
324	980723	05:03	36.74	49.73	13	1.9	60	55	−119	285	44	−54	272	65	170	5	−1	A
326	980723	07:16	36.69	49.82	13	2.5	75	80	45	335	45	165	197	21	305	38	1	A
330	980723	17:30	36.78	49.64	13	2.0	95	82	−20	188	69	−171	49	20	143	8	−1	A
345	980725	12:32	36.69	49.80	12	1.9	220	70	90	40	20	90	310	25	130	65	1	A
350	980725	19:12	36.81	49.75	12	2.9	165	84	89	350	6	95	255	39	74	51	1	B
354	980726	04:53	36.83	49.63	9	2.3	315	75	−46	60	46	−158	266	42	13	18	−1	A
360	980726	19:15	36.69	49.80	12	2.7	130	75	134	235	46	21	188	18	81	42	1	A
362	980726	21:17	36.68	49.82	13	1.9	80	85	179	350	89	0	35	3	304	3	1	A
367	980727	19:44	36.77	49.64	10	1.3	155	80	88	345	10	99	246	35	62	55	1	A

Table 2. (*Continued.*)

N	Date	Time	Lat	Lon	*z*	Mag	Az1	pl1	de1	Az2	pl2	de2	Azp	dep	Azt	det	Im	Q
373	980728	09:40	36.72	49.73	11	2.7	310	70	14	215	76	159	263	4	171	24	1	A
377	980728	22:53	36.73	49.77	16	1.1	355	42	131	125	59	59	236	9	345	61	1	B
382	980730	01:28	36.86	49.60	15	2.2	260	25	90	80	65	90	170	20	350	70	1	A
393	980731	12:43	36.98	49.44	10	2.8	340	32	107	140	59	79	237	14	23	73	1	A
398	980801	16:06	36.85	49.41	11	2.3	300	80	179	30	89	0	255	7	164	7	−1	A

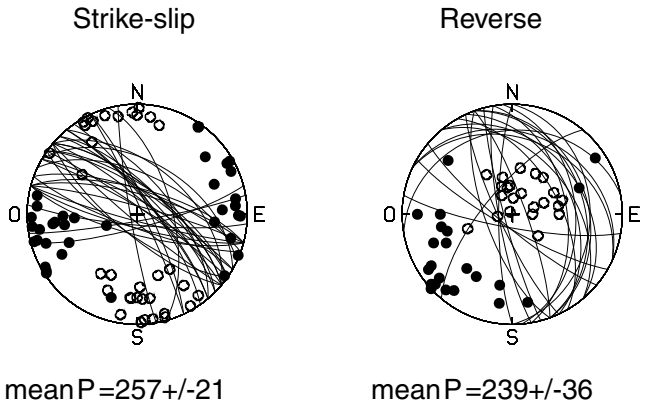

Figure 7. Fault traces, *P*- and *T*-axes of the focal mechanisms. (a) Left-lateral strike-slip mechanisms for which we report only the NW–SE striking plane, (b) reverse mechanisms for which we report the most vertical plane. The inferred active plane trend similarly as well as the mean *P*-axis direction (as for the early aftershocks (Gao & Wallace 1995).

If some of the normal mechanisms are of questionable quality, most of them are well constrained, located at shallow depth, and show mostly ∼NS extension. Some of the reverse mechanisms have nearly vertical and horizontal nodal planes (39, 96, 140, 151, 162, 208, 231, 345, 350 and 367), with the shallow plane dipping generally eastwards (with the exception of 39). The strike-slip mechanisms are mostly left-lateral on a NW–SE trending plane with a few noticeable exceptions (87, 146, and 281). Assuming either left-lateral strike-slip motion on a NW–SE trending plane or reverse motion on a nearly vertical plane, we report the plane direction, as well as the *P*- and *T*-axes on a single stereo equal-area net (Fig. 7). For the strike-slip mechanisms, the mean fault orientation is 304° ±21° and the *P*-axis orientation is 257°+/−21°, very similar to 322°+/−35° and 242°±36°, respectively for the reverse mechanisms. These directions compare well (Table 3) with the early aftershocks mechanisms (Gao & Wallace 1995). The similarity in the orientation of the inferred active plane and the *P*-axes for reverse and strike-slip mechanisms supports a partitioning mechanism.

Table 3. Mean directions of the active fault plane and *P*-axis direction for different sets of mechanisms.

Mechanisms	Az of the fault plane	Az of *P*-axis
Microearthquakes		
Left-lateral strike-slip	304 ± 21	257 ± 21
Reverse	322 ± 35	242 ± 36
Main shock	288	243
Early aftershocks		
Strike-slip	285	239
Reverse	304	236

Cross-sections

To better visualize the geometry of the seismicity with depth, and in an attempt to see whether the microearthquakes are located on or near known major faults, and to infer their motion, we computed eight NE–SW sections (Fig. 8, sections A–H), each with a width of 5 km, striking perpendicular to the surface ruptures, across the active area to see if any particular fault dominates the seismicity.

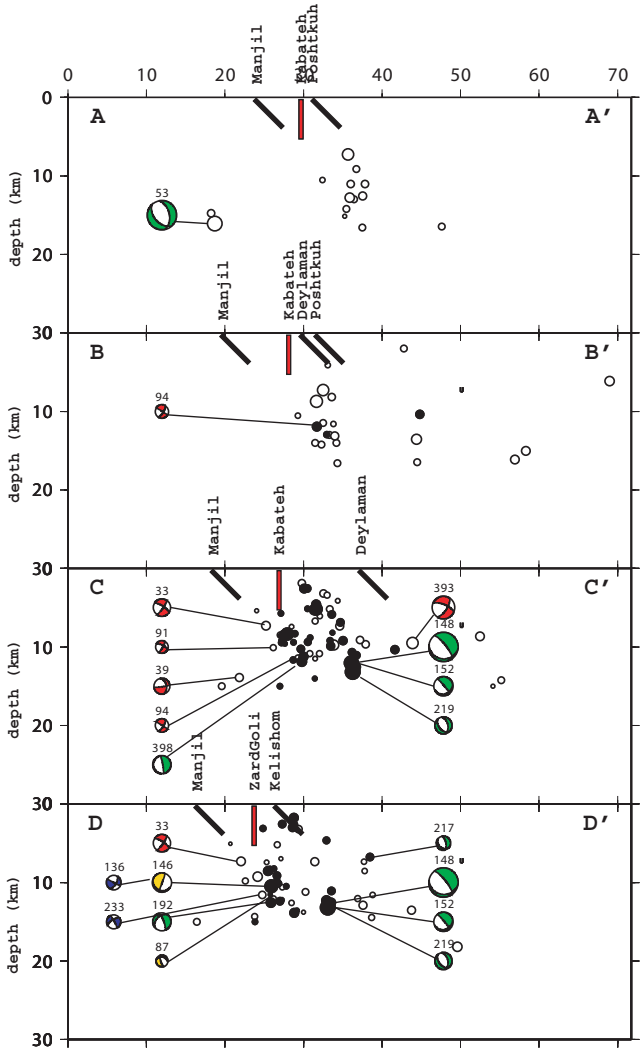

Figure 8. Cross-sections. The width of the section is 5 km which could produce a slight overlap. We report all events as empty circles and selected events (see caption 3) as filled circles. The focal mechanisms projected are equal area projected onto the back hemisphere. Green balloons are left-lateral strike-slip mechanisms, red are reverse, blue are normal and orange are other strike-slip. The locations of the known surface faults are shown by bold lines with the dip polarity proposed by Berberian *et al*. (1992). The 1990 surface ruptures (Berberian *et al*. 1992) are shown by a red line.

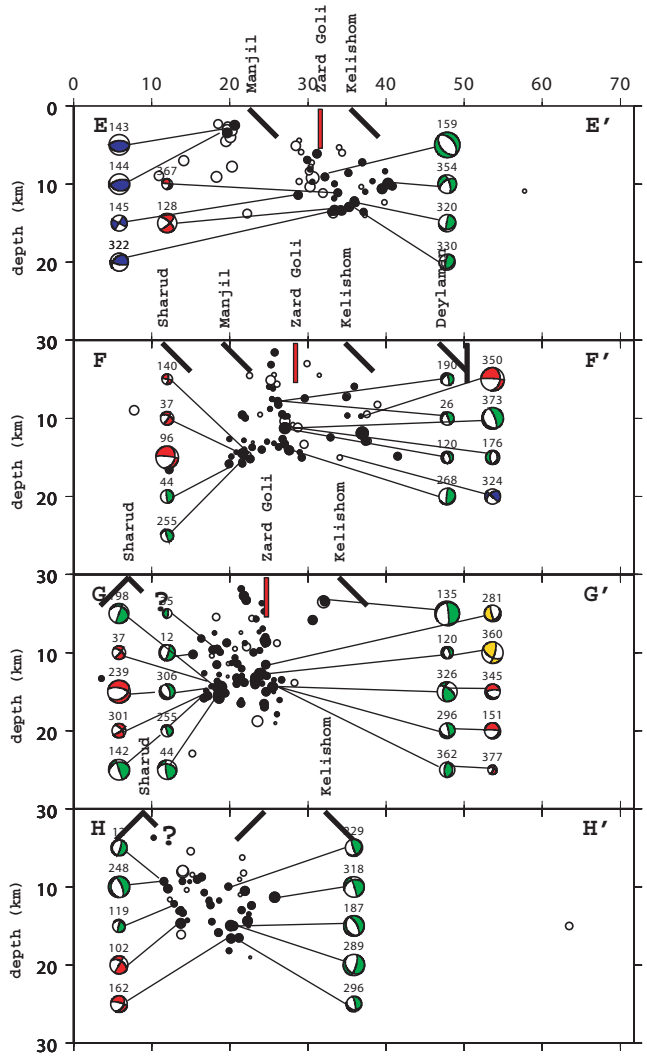

Figure 8. (*Continued.*)

In all sections, we report the seismicity and the focal mechanisms and at surface the faults and their associated dip as mapped by Berberian *et al*. (1992). Microseismicity (especially 8 yr after the main shock) could represent only the diffuse state of stress around the fault system. However, it gives a detailed information that could be interpreted in the frame of the surface tectonics and of the main shock parameters.

The Kabateh fault is associated with a rather simple pattern of seismicity which is aligned almost parallel to the rupture and located slightly north (Figs 3 and 4). The seismicity defines a cluster restricted between 7 and 15 km depth (Figs 5 and 8). But contrary to surface observations suggesting that the Kabateh fault dips steeply SSW (Berberian *et al*. 1992), the aftershock seismicity is located slightly north of the surface rupture. Because the network did not cover this part of the fault, only a few events have an azimuth gap less than 180° and belong to the selected set of best-located events. It is, therefore, uneasy to decide if microseismicity is related to the Kabateh fault dipping vertically or to the Manjil fault dipping north. A plane passing through Manjil has the advantage of being continuous with the dip of the seismicity observed in the sections located further east (Fig. 8; sections C-C′ and D-D′). We have only two focal mechanisms in the area of the Kabateh fault. One strike-slip mechanism in section A (53) is located 20 km south of the fault and unrelated to the Kabateh rupture. Another one (94) is a reverse mechanism with a dipping plane which fits the Manjil fault. An attempt to compute a composite fault plane solution for the 11 earthquakes located on the Kabateh fault having more than eight polarity readings does not help to infer the motion of the Kabateh fault. We propose that the westernmost microseismicity is associated rather with the reverse Manjil fault dipping 45° northwards than with the vertical Kabateh fault.

Section C-C′ (Fig. 8a) is located between the Kabateh and Zard-Goli segments across the dense cluster of activity with both reverse and strike-slip mechanisms. Actually, we distinguish two clusters of activity dipping northwards. The southernmost cluster is not very well defined but is possibly connected to the Manjil fault (which did not break during the main shock). The associated focal mechanisms are both reverse (33, 91 and 94) and strike-slip (398). The northernmost cluster, which extends between the surface and a depth of 15 km and dips ∼45°–60°, is associated with three strike-slip mechanisms (148, 152 and 219) and is likely to be related to the Kabateh rupture or to the Kelishom fault which are very close at that place.

Section D-D′ (Fig. 8) is located at the western termination of the Zard-Goli rupture. The seismicity is quite spread in this section. However, it suggests that some activity could be related to the Manjil fault dipping north with an angle of 45°. Some activity is also located north of the Zard-Goli rupture or the Kelishom faults. Focal mechanisms along the southern fault (Manjil) are a mixture of strike-slip (192), reverse (33), but also normal (136 and 233) mechanism with no clear differentiation with depth. The northern fault is associated only with four strike-slip mechanisms (148, 152, 217 and 219).

Section E-E′ (Fig. 8) is located in the middle of the Zard-Goli rupture. Some shallow activity, at least for the well-located events, is located south of the Manjil fault and is associated with two normal mechanisms (143 and 144). Further north we observe two clusters of activity. The one which seems to be related to the Manjil fault is dipping at 45° northwards. It is associated with several mechanisms which are mostly strike-slip (159, 320 and 330) but a few are reverse (128 and 367) and normal faults (145 and 322). The other cluster, less defined, could connect at the surface to the Zard-Goli rupture and dips north also at 45°. The only mechanism (354) associated with the second cluster is strike-slip. Because the strike of the Manjil and Zard-Goli faults differs from the one of the Kelishom fault, we computed another section perpendicular to the Kelishom fault which confirms that the two active faults are Manjil and Zard-Goli both dipping at 45° north. No activity seems to be related to the Kelishom fault.

Section F-F′ (Fig. 8b), located east of Zard-Goli, shows a more complex pattern. Seismicity is spread between the Manjil fault and the Zard-Goli rupture (Figs 3 and 4). There is a cluster located at ∼15 km depth, which cannot be related to the Manjil fault because it is located exactly underneath. Two reverse (37 and 140) and two strike-slip (44 and 255) mechanisms are associated with this cluster. Further north, a vertical cluster of activity is located immediately underneath (or slightly south of) the Zard-Goli rupture from the surface to 15 km depth; it is associated only with strike-slip mechanisms (26, 120, 176, 190, 268 and 373). A third cluster is located north of the Zard-Goli rupture, beneath the Kelishom fault, and is associated with one dip-slip mechanism (350). If associated with an active fault, it is tentative to relate the southern cluster to the reverse Shahrud fault dipping northwards and not southwards as mapped by Berberian *et al*. (1992). However, the Shahrud fault is located south of the valley and, therefore, a north dipping fault is

inconsistent with geomorphology. The vertical cluster is associated with the strike-slip Zard-Goli rupture dipping vertically in this section. The northernmost cluster is probably associated with the Kelishom fault. Again, we computed a section trending perpendicular to the Kelishom fault which helps to determine that (1) seismicity is located north of the Shahrud fault, (2) earthquakes are located vertically underneath the Zard-Goli rupture and (3) seismicity dips north of the Kelishom fault.

Section G-G′ (Fig. 8) is located east of the termination of the Manjil fault which bends northwards at that place. The interpretation is very similar to that of the previous section but the Manjil fault does not exist at that place. There is a cluster located between Shahrud and Zard-Goli. It is associated mostly with six strike-slip mechanisms (12, 44, 142, 198, 255 and 306) and three reverse mechanisms (37, 239 and 301). Another cluster is located beneath the Zard-Goli rupture and dips almost vertically, again from the surface to 18 km depth. It is associated mostly with strike-slip mechanisms (120, 296, 326, 306 and 362) two right-lateral strike-slip (281 and 360) and three reverse (151, 345 and 377). The section suggests that the southern cluster is again associated with the reverse Shahrud fault dipping north, not south, at 45° and that the northern cluster is associated with the vertical strike-slip Zard-Goli rupture.

Section H-H′ (Fig. 8b) confirms this pattern of two clusters, one dipping 45° north and associated both with reverse (102 and 162) and strike-slip (12, 119 and 248), the other vertical and associated mostly with strike-slip mechanisms (187, 229, 289, 296 and 318).

In summary, even slightly confused, the northern clusters are mainly associated with strike-slip mechanisms whereas the southern clusters are associated with both strike-slip and reverse mechanisms. Although we cannot identify precisely individual major faults, this pattern of mechanisms suggests that the Zard-Goli rupture is likely a strike-slip fault whereas the Manjil fault is more complex, showing both reverse and strike-slip motions.

DISCUSSION

Indeed, as said before, microearthquakes are related to small faults and, therefore, could be related to local (heterogeneous) stress-release rather than to the motion on the main fault. This small-scale energy release could explain the diffuse pattern of seismicity as well as the large variety of mechanisms. However, the comparison between the early aftershock mechanisms (of magnitude greater than 4.6) is consistent with our small mechanisms suggesting that complexity is inherent to this earthquake and to the associated faulting. Moreover, the seismicity pattern (especially in cross-sections) is consistent, on average, with one plane of the focal mechanisms.

Active faults

The seismicity recorded 8 yr after the Rudbar-Tarom earthquake is significant, with ∼400 events (of magnitude up to 4) over 7 weeks. Furthermore, the aftershock activity in 1998 trends WNW–ESE and is concentrated near the two easternmost segments that broke during the main shock, as in 1990 (Niazi & Bozorgnia 1992; Hamzehloo *et al*. 1997a). Most of the seismicity is located north of the fault ruptures, indicating a probable north dipping fault contrary to the inferred (from surface observations) steep southward dip of the various segments during 1990 described by Berberian *et al*. (1992), but more consistent with the vertical plane inferred from the main shock mechanism.

The lack of seismicity associated with the Baklor rupture is not due to the poor coverage of the seismological network deployed mainly above the Kabateh and Zard-Goli ruptures. If this fault was very active, we would not miss earthquakes, or mislocate them so much, because the Baklor fault is located only 20 km west of the seismological network and we recorded and located earthquakes north of the fault at a similar distance. During the 1990 sequence, this part of the fault was also less active than the central part (Gao & Wallace 1995) and experienced less energy release (Campos *et al*. 1994).

We suspect the Kabateh rupture also to have become relatively aseismic. Seismicities in sections A–C do not show an obvious relation with the vertical Kabateh fault, but instead shows a possible relation with the Manjil fault dipping 45° northwards and is associated with both reverse and strike-slip mechanisms. The Manjil fault stops at section F and at that place may step to another reverse fault also dipping 45° northwards, possibly the Shahrud fault.

The Zard-Goli rupture region is more active and complex. Two dense clusters of earthquakes are observed, one between the Kabateh and Zard-Goli segments and the other one at the eastern termination of the fault rupture. These two clusters were also observed during the 1990 sequence (Berberian *et al*. 1992; Gao & Wallace 1995) in a place where no surface ruptures exist. This association between an increase of seismicity (i.e. a region where stresses are not totally released) and discontinuities in the fault rupture is common for aftershocks and is usually related to heterogeneities along the fault. These heterogeneities are either geometrical (a change in the fault geometry or a spreading of the main fault into secondary faults) or rheological barriers (change in the mechanical properties) along the fault. The cluster of seismicity between the Kabateh and Zard-Goli ruptures is associated with the Sefid-Rud river, which completely crosses the Alborz mountains and, therefore, may be related to a NS structural discontinuity (Berberian *et al*. 1992), especially if we assume that the four strike-slip mechanisms (148, 152, 219 and 398) are right-lateral motion on a NE striking plane. Focal mechanisms in this region show a mixture of both reverse faulting (22 mechanisms, *P*-axis trending NE–SW) and strike-slip faulting (38 mechanisms). The Zard-Goli rupture is associated mostly with strike-slip mechanisms, and the aftershock zone beneath it dips 45° northwards in its western part (sections C–E) but vertically in its eastern part (sections F–H).

We can summarize our results as follows:

In the west, the Baklor and the Kabateh faults had few earthquakes at the time of our survey and the seismicity may be related to the Manjil fault dipping 45°, associated mostly with reverse motion. The Manjil fault might be relayed to the east by the Shahrud fault dipping also northwards.

For the Zard-Goli rupture, the pattern is much more complex, but looking at the cross-sections and assuming a minimum of continuity between all of them, we propose an explanation: in the west, the Zard-Goli rupture dips at 45° northwards, but it is vertical in the east. Both sections are mostly associated with strike-slip mechanisms. Finally, no activity is related either to the Kelishom or to Deylaman fault.

A possible fault system

Our observations based on local seismicity recorded 8 yr after the main shock show a complex fault system for the Rudbar-Tarom earthquake (Fig. 9). This complexity was already suggested from the study of the main shock showing three main strike-slip subevents with slightly different mechanisms by Campos *et al*. (1994). In their study, no reverse mechanism, associated with any subevent,

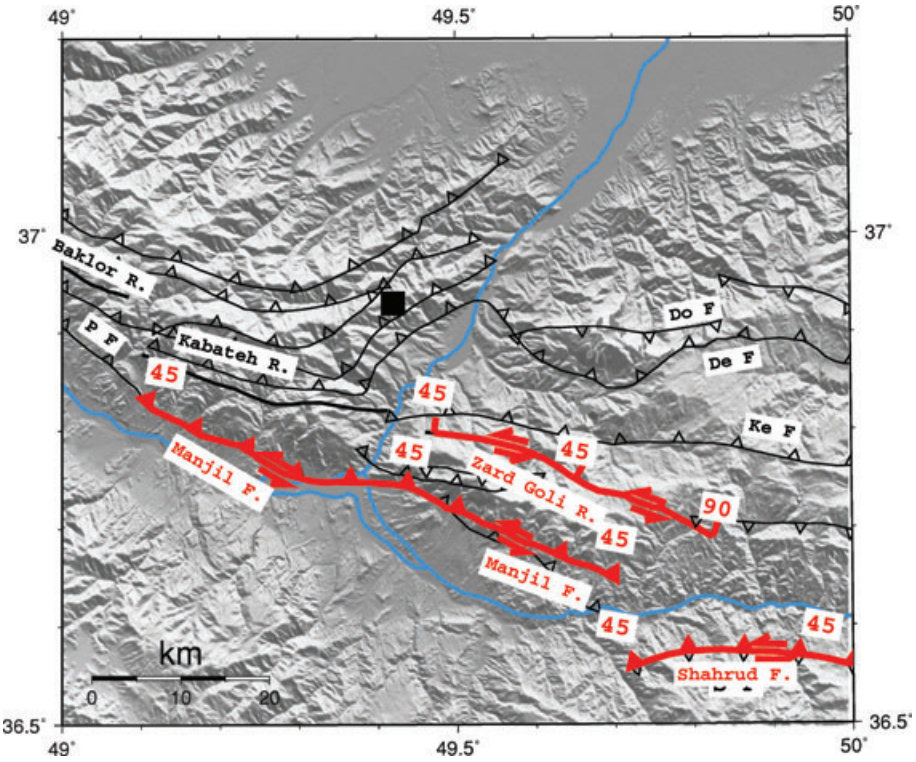

Figure 9. Sketch summarizing our results. We plot in black the existing faults and in purple the active faults (with their dip) deduced form our microseismicity. The Baklor and Kabateh ruptures are not active. The Zard-Goli rupture is associated with a strike-slip fault which dips at 45° northwards to the west and is vertical to the east. The Manjil fault is active with both strike-slip and reverse motions. The Shahrud fault is a relay of the Manjil fault dipping north.

indicated that part of the energy was released on a reverse fault; but the bilateral rupture could obscure possible differences in rupture mechanism between the western and the eastern subevents. The aftershock mechanisms recorded a few days after the main shock show, by contrast, a mixture of strike-slip and reverse faulting (Berberian *et al*. 1992; Gao & Wallace 1995), but the locations of these aftershocks were not precise enough to determine to which fault they belonged.

The centroid mechanism (Gao & Wallace 1995) is the mechanism of the maximum of energy release. The maximum energy (∼60 per cent) of the main shock was released more than 20 s after the rupture initiation, about 40 km east of the epicentre, and therefore probably on the Zard-Goli rupture. In this part, the 1998 microseismicity suggests a fault plane dipping almost vertically, with a majority of the focal mechanisms showing strike-slip, consistent with the main shock. The centroid mechanism is, therefore, likely to be dominated by the vertical strike-slip fault to the east.

Our study suggests that both the Baklor and Kabateh ruptures were not associated with seismicity 8 yr after the main shock. Instead, microseismicity appears to be related to the reverse Manjil fault dipping northwards, which did not break in the main shock. We have observed such an absence of correlation between the main fault and the surface ruptures for several strong events, including the 1995 Kozani (Greece) earthquake (Hatzfeld *et al*. 1997) and the 2003 Bam (Iran) earthquake (Tatar *et al*. 2005), for which ruptures at surface did not align with aftershock zones at depth. Because of the mechanical properties of the shallowest part of the crust, where the rupture is apparently steeper, and because no earthquakes were recorded at depth shallower than 5 km, it is difficult to associate the aftershocks and the surface rupture, and to map a change of fault dip with depth.

Partitioning

At a regional scale, partitioning was proposed to explain the strike-slip mechanism of the 1990 Rudbar earthquake (Berberian *et al*. 1992; Jackson 1992; Gao & Wallace 1995). The average GPS motion between Central Iran and the Caspian shore is small. Across the Central Alborz (52°E), the present-day GPS motion is transpressive with an NS shortening of 5 mm yr^{-1} and a left-lateral shear of 4 mm yr^{-1} (Vernant *et al*. 2004b). In the western Alborz, the deformation pattern becomes more complex. The Tabriz fault accommodates ∼8 mm yr^{-1} of right-lateral motion but GPS measurements suggest that the Talesh mountains accommodate ∼8 mm yr^{-1} of NE extension and the motion in the area of Roudbar is ∼3 mm yr^{-1} of left-lateral trans-tensional motion (Masson *et al*. 2006).

An issue is then to distinguish whether the large vertical strike-slip fault (Zard-Goli) crosses a shallower dipping reverse fault (Manjil) or the opposite. We summarize in Fig. 10 the main characteristics of our results. In sections A and B, we see reverse activity likely related to the Manjil fault only, and no evidence of activity related to the Kabateh rupture. In sections C–D, we see again reverse activity associated with the Manjil fault and strike-slip activity related to a steeper (but not vertical) fault (the Kabateh or Zard-Goli rupture) located in the hangingwall and joining the Manjil fault at 15–18 km depth. Section E, located at the eastern termination of the Manjil fault, is the most complex because we observe normal faulting ahead of the Manjil fault, reverse faulting associated with the Manjil fault, and steep strike-slip faulting in the hangingwall stopping at the Manjil fault. Section F shows a different pattern because the reverse faulting seems impossible to associate with the Manjil fault that would dip too steep, but rather to a fault located south of it, and the Shahrud fault, with reverse polarity, is a good

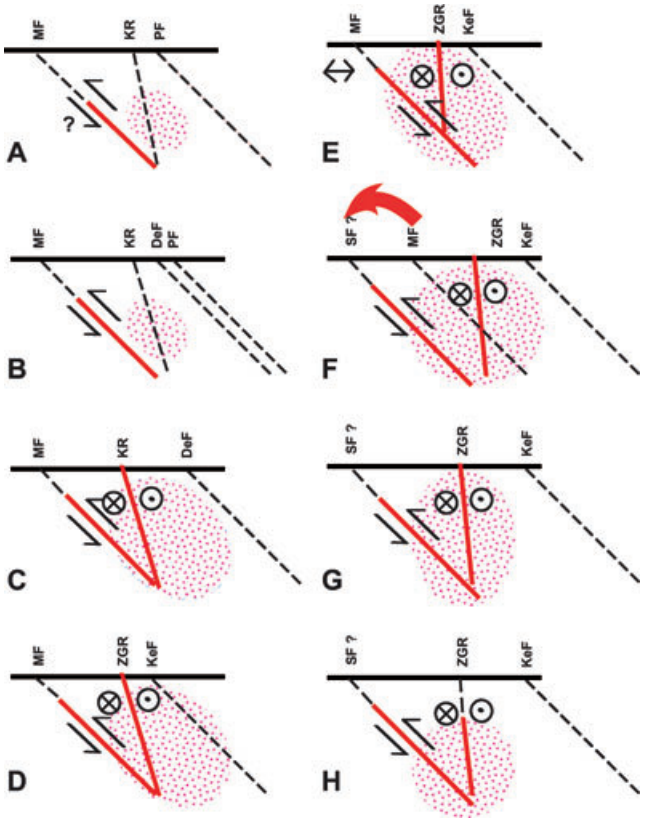

Figure 10. Interpretative summary of the cross-sections based on the seismicity and mechanisms. To the west (sections A–B), reverse faulting is associated to the Manjil fault. In the centre (sections C–D), reverse faulting is associated with the Manjil fault and strike-slip faulting with the Kabateh or Zard-Goli fault dipping north without crossing. Further east (sections E–F), the Zard-Goli becomes vertical and both faults may offset each other which does not allow partitioning of large motion and may be an unstable mechanism. The reverse fault jumps southwards to prevent the strike-slip fault to intersect the strike-slip fault. We observe this jump to the east which is less mature than the west part of the fault. In red, the active faults evidenced by the microseismicity. The dotted areas show the seismicity.

candidate. The strike-slip Zard-Goli fault is almost vertical. This is again particularly clear in sections G–H with the reverse faulting associated with the Shahrud and the vertical strike-slip faulting associated with Zard-Goli.

Therefore, for the western sections A–E, the partitioning is between the reverse Manjil fault and the strike-slip Kabateh and Zard-Goli faults located in the hangingwall. When the distance between the two reverse and strike-slip faults is too small, as in section F, the reverse fault jumps southwards (possibly to the Shahrud fault), rather than having strike-slip faulting located in the footwall and crossing the reverse fault. Further east, in sections G–H, we still observe partitioning not anymore on the Manjil fault, but on another fault located southward.

We think that we have, in these sections, an evidence that the vertical strike-slip motion does not cross the reverse fault at depth. When the space is too small, the reverse fault jumps away to keep possible large motion on both faults.

The difference between the western and the eastern part of the sections is likely due to a difference in maturity of both sides of the fault. If true, this explain why most of the energy release was associated with the less mature eastern part of the fault whereas, at surface, the western part seems more developed.

CONCLUSIONS

The Rudbar-Tarom earthquake was unexpected because no strong earthquake has been observed in this area. The left-lateral strike-slip mechanism was also unexpected because it did not fit into the tectonic regime of the western Alborz. Three segments are supposed to have broken during the main shock and three rupture segments, unrelated to existing faults, were observed at surface. Partitioning on two faults close from each other was proposed to explain the mechanism, but the faults and their geometry involved in the partitioning were speculative.

Our seismological network was installed in 1998 over the two main segments that ruptured in 1990. The results of the microseismicity survey may be blurred because of the progressive damping and diffusion of the local stresses. However, they constrain some of the characteristics of this fault system (Fig. 9).

(1) The depth of the seismicity is restricted between the surface and 20 km with a majority of events located between 8 and 16 km. This is consistent with the centroid depth of 14 km for the main shock (Gao & Wallace 1995) and a fault system restricted to the brittle crust.

(2) A possible barrier between the Kabateh and Zard-Goli segments is located at the Sefi-Rud river which did not experience surface deformation during the main shock and which might play an important structural role.

(3) The different cross-sections show a mixture of reverse and strike-slip faulting. On the western part, partitioning between the reverse Manjil fault and a steep strike-slip fault related to the Kabateh rupture explains the seismicity. Further east, after a complex transition, the distance between the reverse and the strike-slip Zard-Goli fault is not large enough to accommodate large motion. The reverse fault jumps, therefore, southwards to make room to the strike-slip fault which cannot cross the Manjil reverse fault to keep the motion stable.

ACKNOWLEDGMENTS

This work was supported by International Institute of Earthquake Engineering and Seismology (IIEES), INSU-CNRS (Programme Intérieur de la Terre) and the French Ministère des Affaires Etrangères in the frame of a cooperative research programme between France en Iran. We thank M. Ghafory-Ashtiany, president of IIEES, for his encouragements. We thank both IIEES and LGIT staffs for support, administrative and field work assistance. We also thank K. Alizadeh, D. Brito, A. Fahtehi, P. Guéguen, A. Kaviani. M. Massoudi, J. Noir, F. Yamini-Fard, M. Zolfaghari for their help in the field work. This study would not have been possible without help of people and especially the government staff of Gilan province. Comments from J. Jackson and a tenacious anonymous reviewer greatly helped to improve the manuscript.

REFERENCES

Alavi, M., 1996. Tectonostratigraphic synthesis and structural style of the Alborz mountain system in northern Iran, *J. Geodyn.,* **21,** 1–33.

Allen, M.B., Ghassemi, M.R., Sharabi, M. & Qoraishi, M., 2003. Accommodation of late Cenozoic oblique shortening in the Alborz range, northern Iran, *J. Struct. Geol.,* **25,** 659–672.

Ambraseys, N.N. & Melville, C.P., 1982. *A History of Persian Earthquakes, Cambridge Earth Science Series,* Cambridge University Press, London.

Ashtari, M., Hatzfeld, D. & Kamalian, N., 2005. Microseismicity in the region of Tehran, *Tectonophysics,* **395,** 193–208.

Axen, G.J., Lam, P.S., Grove, M., Stockli, D.F. & Hassanzadeh, J., 2001. Exhumation of the west-central Alborz Mountains, Iran, Caspian subsidence, and collision-related tectonics, *Geology,* **29,** 559–562.

Berberian, M., 1994. Natural hazards and the first earthquake catalog of Iran, Vol. 1: historical hazards in Iran prior 1900, I.I.E.E.S. report.

Berberian, M. & Yeats, R.S., 1999. Patterns of historical earthquake rupture in the Iranian plateau, *Bull. seism. Soc. Am.,* **89,** 120–139.

Berberian, M. & Yeats, R.S., 2001. Contribution of archaeological data to studies of earthquake history in the Iranian plateau, *J. Struct. Geol.,* **23,** 563–584.

Berberian, M., Qorashi, M., Jackson, J.A., Priestley, K. & Wallace, T., 1992. The Rudbar Tarom earthquake of 20 June 1990 in NW Persia: preliminary field and seismological observations and its tectonic significance, *Bull. seism. Soc. Am.,* **82,** 1726–1755.

Campos, J., Madariaga, R., Nabelek, J., Bukchin, B.G. & Deschamps, A., 1994. Faulting process of the 1990 June 20 Iran earthquake from broadband records, *Geophys. J. Int.,* **118,** 31–46.

Engdahl, E.R., Van Der Hilst, R. & Buland, R., 1998. Global teleseismic earthquake relocation with improved travel times and procedures for depth determination, *Bull. seism. Soc. Am.,* **88,** 722–743.

Engdahl, E.R., Jackson, J.A., Myers, S.C., Bergman, E.A. & Priestley, K., 2006. Relocation and assessment of seismicity in the Iran region, *Geophys. J. Int.,* **167,** 761–778.

Fitch, T., 1972. Plate convergence, transcurrent faults, and the internal deformation adjacent to Southeast Asia and the Western Pacific, *J. geophys. Res.,* **77,** 4432–4460.

Gao, L. & Wallace, T.C., 1995. The 1990 Rudbar–Tarom Iranian earthquake sequence: evidence for slip partitioning, *J. geophys. Res.,* **100,** 15 317–15 332.

Hamzehloo, H., Sarkar, I. & Chander, R., 1997a. Analysis of some aftershocks of the Rudbar earthquake of 1990 using Master event technique, *Bull. Ind. Soc. Earth. Tech.,* **34,** 1–15.

Hamzehloo, H., Chander, R. & Sarkar, I., 1997b. Probable role of the Sefirud Reservoir in the occurrence of the Rudbar earthquake of 1990, *Bull. Ind. Soc. Tech.,* **34,** 17–25.

Hatzfeld, D. *et al*., 1997. The Kozani-Grevena earthquake of May 13, 1995. A seismological study, *Bull. seism. Soc. Am.,* **87,** 463–473.

Jackson, J., 1992. Partitioning of strike-slip and convergent motion between Eurasia and Arabia in Eastern Turkey and the Caucasus, *J. geophys. Res.,* **97,** 471–479.

Jackson, J., Priestley, K., Allen, M. & Berberian, M., 2002. Active tectonics of the south Caspian basin, *Geophys. J. Int.,* **148,** 214–245.

Jones, R.R. & Tanner, P.W.G., 1995. Strain partitioning in transpression zones, *J. Struct. Geol.,* **17,** 793–802.

Jones, C.H. & Wesnousky, S.G., 1992. Variation in strength and slip rate along the san Andreas fault system, *Science,* **256,** 83–86.

Kissling, E., 1988. Geotomography with local earthquake data, *Rev. Geophys.,* **26,** 659–698.

Langston, C.A., 1979. Structure under Mount Rainier,Washington, inferred from teleseismic body waves, *J. geophys. Res.,* **84,** 4749–4762.

Lettis, W.R. & Hanson, K.L., 1991. Crustal strain partitioning: implications for seismic-hazard assessment in western California, *Geology,* **19,** 559–562.

Liggoria, J.P. & Ammon, C., 1999. Iterative deconvolution and receiver function estimation, *Bull. seism. Soc. Am.,* **89,** 1395–1400.

Mangino, S. & Priestley, K., 1998. The crustal structure of the southern Caspian region, *Geophys. J. Int.,* **133,** 630–648.

Masson, F., Djamour, Y., van Gorp, S., Chéry, J., Tatar, M., Tavakoli, F., Nankali, H. & Vernant, P., 2006. Extension in NW Iran driven by motion of the South Caspian Bosin, *Earth Planet. Sc. Lett.,* **252,** 180–188.

McCaffrey, R., 1992. Oblique plate convergence, slip vctors, and forearc deformation, *J. geophys. Res.,* **97,** 8905–8915.

McKenzie, D. & Jackson, J., 1983. The relationship between starin rates, crustal thickening, paleomagnetism, finite strain and fault movements within a deforming zone, *Earth planet. Sci. Lett.,* **65,** 182–202.

Michael, A.J., 1990. Energy constraints on kinematic models of oblique faulting: loma Prieta versus Parkfield-Coalinga, *Geophys. Res. Lett.,* **17,** 1453–1456.

Moinfar, A.A. & Naderzadeh, A., 1990. An immediate and preliminary report on the Manjil, Iran earthquake of 20 June 1990, Building and Housing Research Center, Ministry of Housing and Urban Development 119, 68 pp.

Molnar, P., 1992. Brace-Goetze strngth profiles, the partitioning of strike-slip and thrust faulting at zones of oblique convergence, and the stress-heat flow paradox of the San-Andreas Fault, in *Fault Mechanics and Transport Properties of Rocks,* pp. 435–459, eds Evans, B. & Wong, T.-F., Academic Press, London.

Mount, V.S. & Suppe, J., 1987. State of stress near the San Andreas fault: implications for wrench tectonics, *Geology,* **15,** 1143–1146.

Niazi, M. & Bozorgnia, Y., 1992. The 1990 Manjil, Iran, Earthquake: Geology and seismology overview, PGA attenuation, and observed damage, *Bull. Seis. Soc. Am.,* **82,** 774–799.

Norris, R.J. & Cooper, A.F., 2001. Late Quaternary slip rates and slip partitioning on the Alpine Fault, New Zealand, *J. Struct. Geol.,* **23,** 507–520.

Richard, P. & Cobbold, P., 1989. Structures en fleur positives et décrochements crustaux: modélisation analogique et interprétation mécanique, *C. R. Acad. Sci. Paris,* **308,** 553–560.

Sodoudi, F., Kind, R., Kamalian, N. & Sadidkhoy, A., 2004. The crustal and upper structure of the Central Alborz using teleseismic receiver functions, in *European Geosciences Union 1st General Assembly,* Nice, 25–30 April, 2004.

Stöcklin, J., 1974. Possible ancient continental margin in Iran, in *Geology of Continental Margins,* pp. 873–877, eds Burke, C. & Drake, C., Springer-Verlag, New York.

Tatar, M., 2001. Etude sismotectonique de deux zones de collision continentale: le Zagros Central et l'Alborz (Iran), *Thèse de l'Université de Grenoble*.

Tatar, M., Hatzfeld D. & Ghafory-Ashtiany M., 2004. Tectonics of the Central Zagros (Iran) deduced from microearthquake seismicity, *Geophys. J. Int.,* **156,** 255–266.

Tatar, M., Hatzfeld, D., Moradi, A. & Paul, A., 2005. The 26 December 2003 Bam earthquake (Iran), Mw 6.6, aftershock sequence, *Geophys. J. Int.,* **163,** 90–105.

Tatar, M., Jackson, J., Hatzfeld, D. & Bergman, E., 2007. The 28 May 2004 Baladeh earthquake ($M_w \sim 6.2$) in the Alborz, Iran: implications for the geology of the South Caspian Basin margin and for the seismic hazard of Tehran, *Geophys. J. Int.,* **170,** 249–261.

Teyssier, C., Tikoff, B. & Markely, M., 1995. Oblique plate motion and continental tectonics, *Geology,* **23,** 447–450.

Trifonov, V.G., Hessami, K.T. & Jamali, F., 1996. West-Trending Oblique Sinitral–Reverse Fault system in Northern Iran, Vol. 75, *IIEES Special Pub*., Tehran, Iran.

Vernant, Ph. *et al*., 2004b. Deciphering oblique shortening of central Alborz in Iran using geodetic data, *Earth planet. Sci. Lett.,* **223,** 177–185

Waldhauser, F. & Ellsworth, W.L., 2000. A double difference earthquake location algorithm: method and application to the northern Hayward fault, California, *Bull. seism. Soc. Am.,* **90,** 1353–1368.

Yamini-Fard, F., Hatzfeld, D., Tatar, M. & Mokhtari, M., 2006. Microseismicity on the Kazerun fault system (Iran): evidence of a strike-slip shear zone and a thick crust, *Geophys. J. Int.,* **166,** 186–196.

Zoback, M.D. *et al*., 1987. New evidence on the state of stress of the San Andreas Fault system, *Science,* **238,** 1105–1111.

SUPPORTING INFORMATION

Additional Supporting Information may be found in the online version of this article:

Appendix S1. A zip file containing two supporting figures.

Please note: Wiley-Blackwell are not responsible for the content or functionality of any supporting materials supplied by the authors. Any queries (other than missing material) should be directed to the corresponding author for the article.